OAK RIDGE NATIONAL LABORATORY LIBRARIES
3 4456 0577766 5

International Journal of MATERIALS RESEARCH

Zeitschrift für METALLKUNDE

10/2006

CENTRAL RESEARCH LIBRARY
OCT 25 2006

Dedicated to Professor Dr. Eckard Macherauch
on the occasion of the 80 anniversary of his birth

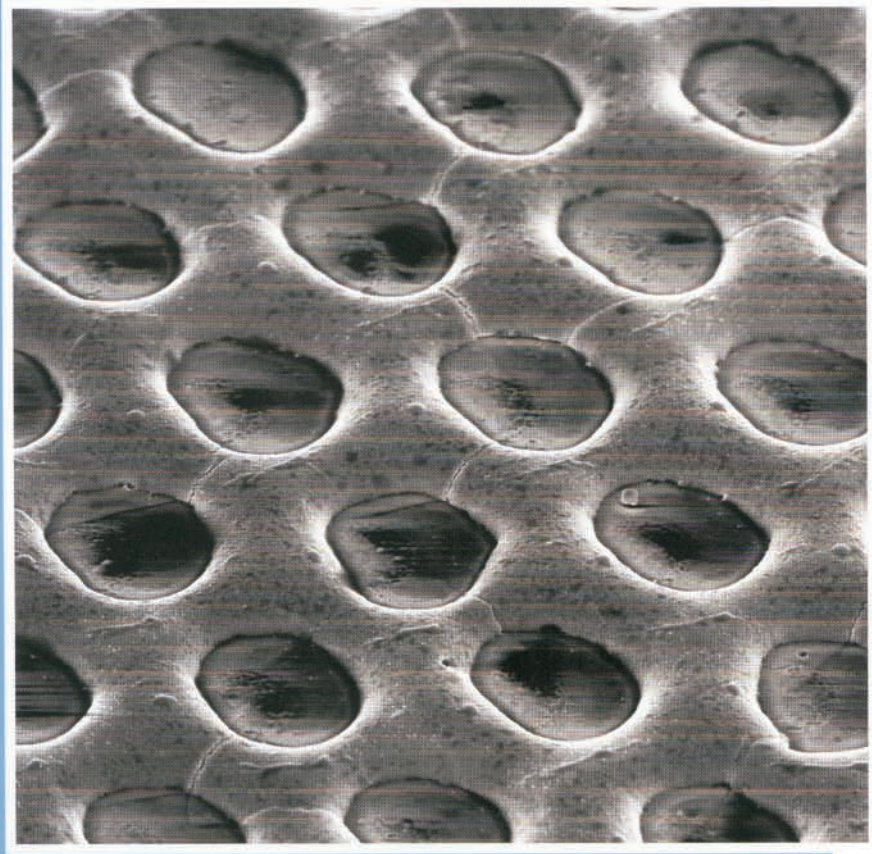

Featured:
F. Mücklich, A. Lasagni, C. Daniel,
Laser Interference Metallurgy – using interference as a tool for micro/nano structuring
pp. 1337-1344

Editor:
Deutsche Gesellschaft für Materialkunde

Managing Editors:
M. Rühle
G. Petzow
P. P. Schepp

Volume 97, October 2006

www.ijmr.de

HANSER

Frank Mücklich[a], Andrés Lasagni[a], Claus Daniel[b]
[a] Department of Materials Science, Saarland University, Saarbrücken, Germany
[b] Materials Science and Technology Division, Oak Ridge National Laboratory, TN, USA

Laser Interference Metallurgy – using interference as a tool for micro/nano structuring

Dedicated to Professor Eckard Macherauch on the occasion of the 80th anniversary of his birth

Interfering laser beams of a high-power pulsed laser provide the opportunity of applying a direct lateral interaction with the surface microstructure of metals in micro/nanoscale based on photo-thermal nature mechanisms. This "Laser interference metallurgy" allows the creation of periodic patterns of features with a well defined long-range order on metallic surfaces at the scale of typical microstructures (from the sub micrometer level up to micrometers). This technique is an approach to initiate metallurgical processes such as melting, recrystallization, recovery, and defect and phase formation in the lateral scale of the microstructure itself and with an additional long range order given by the interference periodicity. In this work, the laser interference theory is described and used to calculate multi-beam interference patterns. A method to calculate the numbers of laser beams as well as the geometrical arrangement of the beams to obtain a desired periodical pattern prior to experiments is presented. The formation of long-range-ordered intermetallic compounds as well as macroscopic and microscopic variations of mechanical properties on structured metallic thin films are presented as examples.

Keywords: Laser interference metallurgy; Intermetallics; Topography; Mechanical properties

1. Introduction

The topography and microstructures of material surfaces strongly influence their properties and even their functions; therefore the creation of well defined regular surface structures may lead to advanced functionalization as well as completely new or enhanced properties [1–3].

Structuring techniques can be basically divided into two groups: (1) methods which require mechanical processes to produce the structure, and (2) methods which utilize beams of electromagnetic waves (e. g. visible light, UV) or particles (e. g. electrons, ions). The first group includes techniques based on printing, molding and embossing making use of a master [4]. The second group includes optical lithography [5], E-Beam lithography [6], laser writing [7], holographic patterning [8] and direct laser interference patterning [9] amongst others.

Direct laser interference patterning [9] uses a single preparation step whereas other holographic methods comprise at least two different steps (irradiation, etching, developing, etc). In addition, in the case of laser interference patterning no masks are required. Relatively large areas can be directly structured (of the order of cm^2) in a time scale of a few seconds. For example, using the direct laser writing technique, about 56 h are required to produce a periodical line-type structure on an area of $3 \times 3\ mm^2$ with a period of 10 µm (using a beam scanning speed of $30\ \mu m \cdot s^{-1}$ [10]). The same structure can be realized in only 10 ns using the direct laser interference patterning technique.

Direct laser interference patterning has been applied in different materials such as semiconductors, metals, ceramics, and polymers [11–18]. In the case of metals, the interference pattern produced by beams of a high-power pulsed laser permits a direct, periodical local heating of the surfaces through the local photo-thermal interaction between laser and metal. In the process of light interaction with metals, the light quanta are absorbed by conducting electrons, which dissipate the absorbed energy as thermal lattice vibrations [19]. Thus, different metallurgical effects such as melting, recrystallization, quenching, recovery, defect or phase formation can be exploited. Therefore, the name Laser Interference Metallurgy (LIMET) was introduced [9].

In this review, we present firstly the interference principle together with the advanced design of periodic patterns by means of the two dimensional Fourier Transformation. Next are shown some results of topographical structuring of thin metallic films. Finally, the lateral formation of intermetallic phases as well as microscopic and macroscopic modulation of mechanical properties are reported as an example.

2. Interference principle

The simplest form of light is a monochromatic, linearly polarized plane wave. This is a sufficient approximation of a real laser beam. Under the assumption of plane waves, the total field (E) of the interference pattern can be obtained by adding all the individual "j" beams [20]:

$$E \quad \sum_{j=1}^{n} E_j = \sum_{j=1}^{n} E_{j0} e^{i(kr-\omega t)} \qquad (1$$

where E_{j0} is the amplitude of the electric field of the j-beam, $\boldsymbol{r}$ is the coordinate along the direction of propagation, ω is the angular frequency, t is the time, and k is the

Table 1. Laser parameters employed to produce the one- and two-dimensional periodical structures shown in Fig. 5. For three laser interference experiments, the angle between the laser beams parallel to the surface sample was 120° (symmetrical configuration). $^{(*)}E_1\%$, $E_2\%$ and $E_3\%$ represent the percentage of the energy of each partial beam relative to the principal beam ($E_1\% + E_2\% + E_3\% = 100\%$) (from [27]).

Sample	Fluence ($mJ \cdot cm^{-2}$)	α_1 (grad)	α_2 (grad)	α_3 (grad)	$E_1\%$ (*)	$E_2\%$ (*)	$E_3\%$ (*)
Fig. 5a	135	2.53	2.53	–	50	50	–
Fig. 5b	65	1.72	1.72	1.72	33.3	33.33	33.33
Fig. 5c	101	1.72	1.72	1.72	33.33	16.66	50.00
Fig. 5d	142	1.83	1.83	1.83	33.33	33.33	33.33

For relative low laser fluences, only the second layer with the lower melting point is molten at the interference maxima positions. The molten material (with a lower density compared with the metal in the solid state, and thus with a larger volume) deforms the upper layer leading to a periodic pattern with a structure depth of the order of the layer thickness. In addition, for metallic systems with very different melting points, the structuring of the samples occurs at lower laser fluences [26]. Examples of the periodical structures formed in this structuring regime are shown in Fig. 5a, b and c [27]. Table 1 shows the angles and the partial energies of the beams employed in each experiment as a percentage of the total energy of the primary laser beam. The examples include structures produced with different geometrical configurations (2 and 3 laser-beam interference experiments) as well as different laser fluences [27]. The experimentally obtained periodical structures are consistent with the calculated interference pattern (see insert in Fig 5a, b and c) and it can be demonstrated that the bumps are located at the interference maxima positions.

In the second case, if the laser fluence is high enough to melt the upper layer as well, the latter is removed at the interference maxima producing a highly structured pattern [28]. Thus, the structuring occurs with removal of material at the energy maxima positions. This is illustrated in Fig. 5d with a crater-type structure obtained in the sample Fe(30 nm)/Al(120 nm). This pattern corresponds to the calculated intensity distribution of Fig. 2b using equation (8)

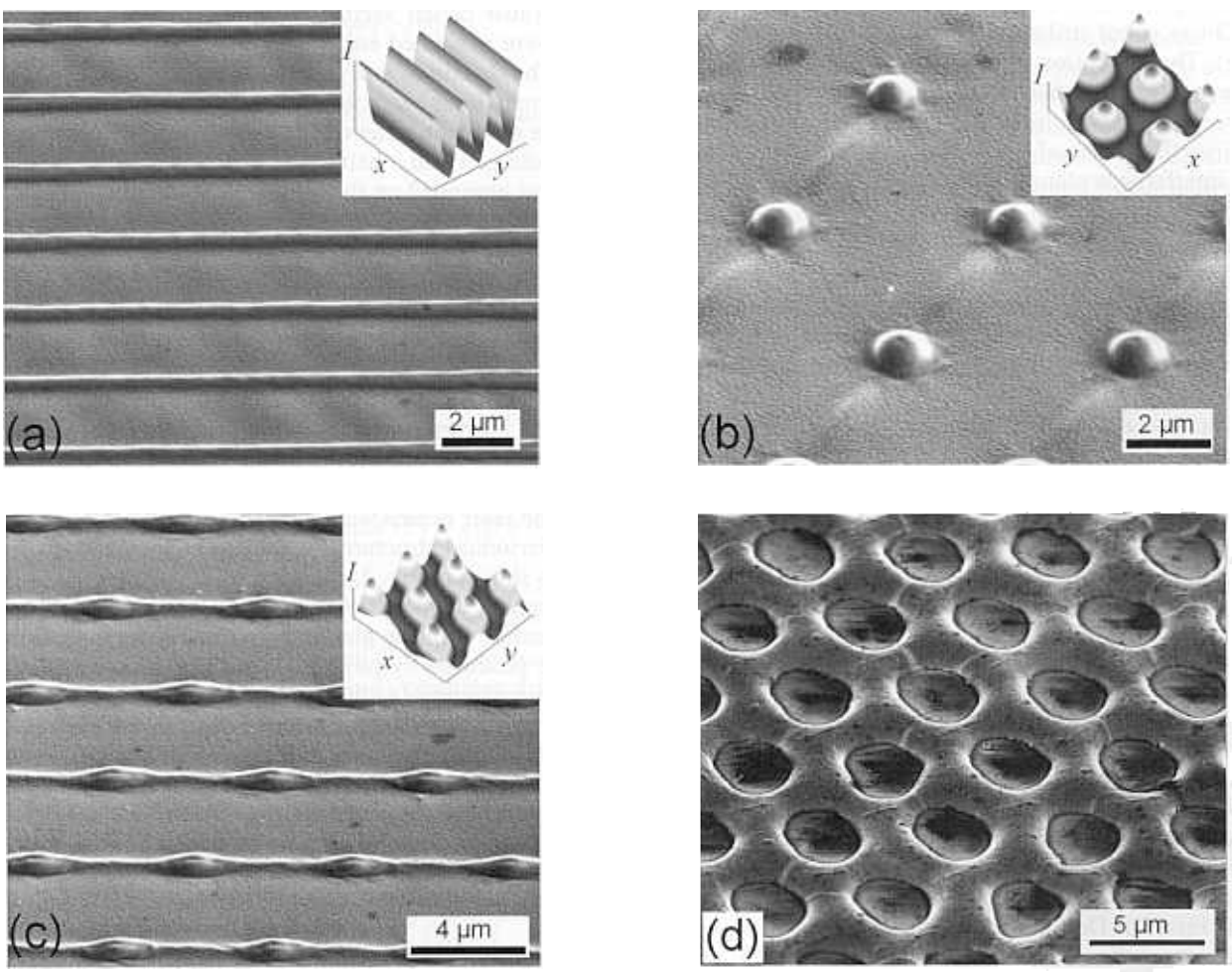

Fig. 5. One- and two-dimensional patterns on Fe(30 nm)/Al(120 nm)/glass sample. The inserts in (a), (b) and (c) show the calculated interference pattern according to [10]. The angle α and the conditions employed to obtain the structures are shown in Table 1. (a), (b) and (c) from [27]; (d) from [20].

with $\alpha = 1.64°$ and $\lambda = 266$ nm resulting in a period of 5.36 μm [20].

From both experiments, it can be concluded that the interference theory can be successfully applied to calculate the geometry of the pattern before irradiation. The topography type obtained will also depend on the laser fluence value, producing a structuring with or without removal of material at the interference maxima positions.

5.2. Two layer systems – Case B: Metal with the lower melting point on top

A second configuration consists also of bi-layered samples, but in this case, the metal with the lower melting point is placed at the top of the sample (sample Al/Fe/glass). For this configuration, three different topography regimes are obtained depending on the laser fluence. The first topography type occurs without removal of material at the interference peaks. In this case, the structure depth is very low compared to the other topography regimes and is explained due to the local thermal dilatation and permanent deformation of the layer. If the laser fluence is high enough so that the Al-layer reaches the melting point, the first transition in the topography regime occurs (see Fig. 6). On the high fluence side of the transition, the Al at the interference peaks is removed but the second layer remains in the solid state. At higher laser fluences, the second layer is also molten resulting in a second transition.

In [20, 25], finite element thermal simulations were used to explain the different topographical regimes which are obtained depending on the laser fluence. The simulation is based on the heat diffusion equation:

$$\rho c_p \frac{\partial T}{\partial t} = q_a - q_m - q_b + \nabla(k\nabla T) \tag{13}$$

where $T = T(x, z, t)$ is the temperature at the position (x, z) at time t, q_a the power per unit of volume added, q_m and q_b the power per unit volume required to melt and vaporize the material respectively, c_p the specific heat, k the thermal conductivity, and ρ the density.

The power of the laser is absorbed into the material following an interference pattern given by:

$$q_a = \alpha \frac{I(x)}{\sigma\sqrt{2\pi}} \exp\left(-\frac{(t - t_p)^2}{2\sigma^2}\right)(1 - r)\exp(-\alpha z) \tag{14}$$

$$\sigma = \frac{\tau_p}{2\sqrt{2\ln 2}} \tag{15}$$

where α is the absorption coefficient, t the time, t_p the pulse time, τ_p the pulse duration (FWHM), r the reflectivity of the surface, and $I(x)$ is the two-dimensional energy per unit of area of the interference pattern described by Eq. (6) (for further details about the simulation method see Refs. [20, 25]).

Figure 7 shows the evolution of the structure depth (experimental), temperature at the interference maxima positions, and molten and vaporized material of the layers (simulated) as a function of the laser fluence for the sample Al(30 nm)/Fe(120 nm) [20]. As can be seen, the transitions of the structure regimes occur when the laser energy is enough to heat one or both layers up to their melting point: the aluminum layer is removed for the laser fluence-range at which the simulation indicates that the aluminum layer is molten and that both layers are removed at the interference maxima positions when both of the layers are molten. These transitions can be seen in Fig. 7 as a sharp increase of the structure depth as a function of the laser fluence and are consistent with the simulation results.

6. Advanced microstructure design

Due to the steep temperature gradient across the interference pattern [29], the process of laser interference structuring can also be used for local phase formation, specifically intermetallics. The intermetallic patterning permits the formation of surface composites and therefore a new kind of

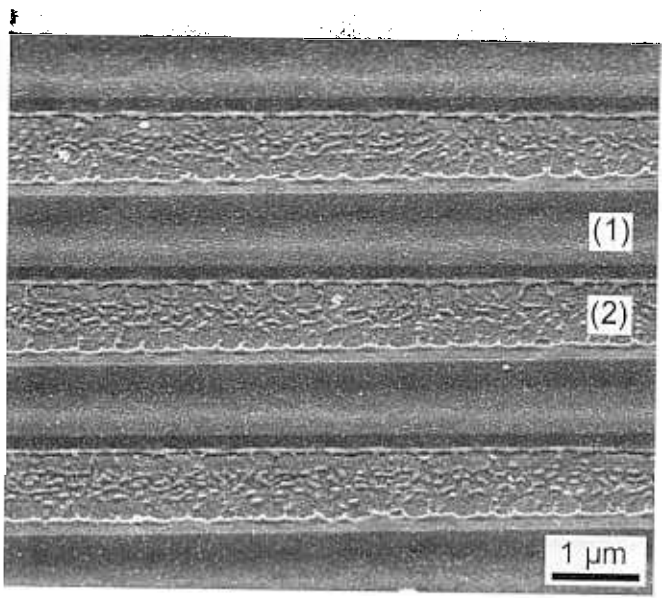

Fig. 6. Resulting line structure with a period of 3.08 μm of an Al(30 nm)/Fe(120 nm) sample. (1) interference minima; (2) interference maxima [20].

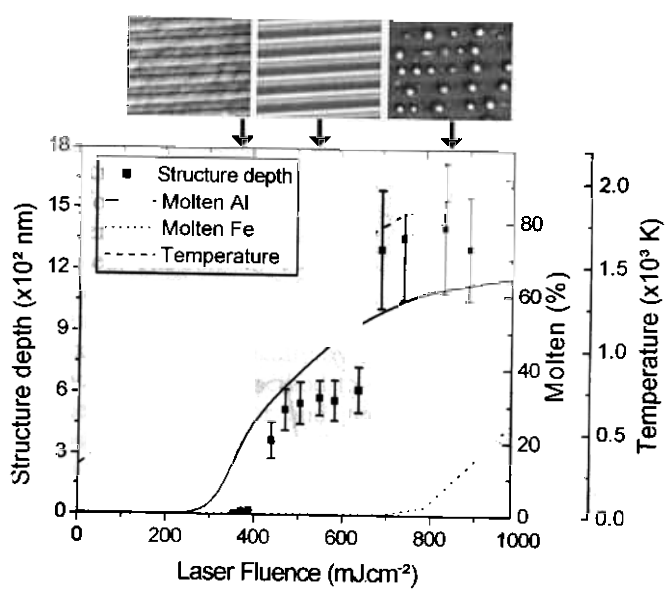

Fig. 7. Structure depth (experimental), temperature, molten and vaporized material (simulated) as a function of the laser fluence for the Al(30 nm)/Fe(120 nm) sample. The details show the topography types obtained in each energy regime: with and without removal of material (optical micrographs) [20].

tailoring of mechanical properties. Three different examples will be presented.

6. Ni_3Al; long range order intermetallic formation

On a substrate (silicon wafer c-Si(100)) a Ni–Al film was deposited with a film thickness of 900 nm at 400 °C by the magnetron sputtering technique. The atomic ratio of the layer was kept 3 : 1 for Ni : Al, which is the stoichiometric ratio for Ni_3Al [30]. X-ray diffraction was applied to prove whether or not an inter-metallic reaction occurred between Ni and Al (for details see [31]).

For characterization of the consequences for the mechanical properties, a nano-indentational AFM was applied to check the local hardness of the structured surface directly within intervals of 200 nm. The hardness in the laser treated area, where laser intensity exceeds a certain threshold level, is significantly higher than that of the area in between, where laser intensity is below this threshold level. The average hardness in the laser treated area is close to 10 GPa, while for the "in between" area it is around 4 GPa, which is close to the untreated state (Fig. 8).

6.2. Grain size distribution, local phases and texture

The microstructural evolution (namely grain size distribution, local phases and texture) of irradiated Ni/Al multi-films was analyzed by TEM measurements to explain the property changes [32]. The sample consisted of twenty Ni/Al bi-layers with a total thickness of around 1 μm. The thickness of each metallic layer was 20.0 and 30.3 nm for Ni and Al, respectively, obtaining an atomic ratio near 1 : 1.

The individual layers in the multi-film show a strong plastic deformation in the area of laser intensity maxima. There is a significant difference in the morphology of the individual Ni and Al layers (see Fig. 9). The Al layers have changed the thickness and layer morphology while the Ni layers are only deformed without any significant thickness change. In the upper two bi-layers, the layer structure is strongly deformed and a zone of inter-diffusion between these layers can be found. This can be explained as follows. The periodic heat treatment activates a periodic melting of the Al layers but leaves the Ni layers in the solid state [25]. Because of the resulting compressive stress induced by periodically and partially molten Al layers during the fast thermal treatment, the Ni layers receive periodic deformation with high velocity (high-speed deformation [33]) which results in work hardening of the Ni films.

The grain sizes are determined by analyzing the size of the bright grains in dark field images generated by different diffracting reflexes. The grain size distribution is statistical but it is grouped in local regions of laser structuring. The unchanged sample regions show grain sizes of about 20 to 30 nm due to the individual layer thickness (see Fig. 9 area 1). The average grain size at the surface (see area 2) is less than 10 nm which was also found by Liu et al. [34] in similar experiments. In the last manipulated Al layer (see area 3) exactly one grain has grown laterally to a size over 100 nm. The cooling rate after melting was calculated to be in the order of 10^{10} K · s^{-1} on the surface [29], but it is not constant and independent on the lateral and vertical coordinates. The grain size changes according to the relative position to the laser interference pattern. Due to the lateral periodicity of the thermal treatment, the local grain size reflects the local cooling rate. In the upper layer in the area of laser intensity maxima, the structure is fine grained (5 to 10 nm, area 2 of Fig. 9). In the lowest deformed Al layer the lower cooling induces lateral grain growth to a size of more than 100 nm (area 3 of Fig. 9) while the grain sizes in the unchanged regions of the sample remain at about 20 to 30 nm, fixed by the individual film thickness (area 1 of Fig. 9). In this way introduced residual compressive stresses can reach values much higher than the yield stress because of the small thickness of 20 nm and 30 nm for the Ni and Al layers, respectively.

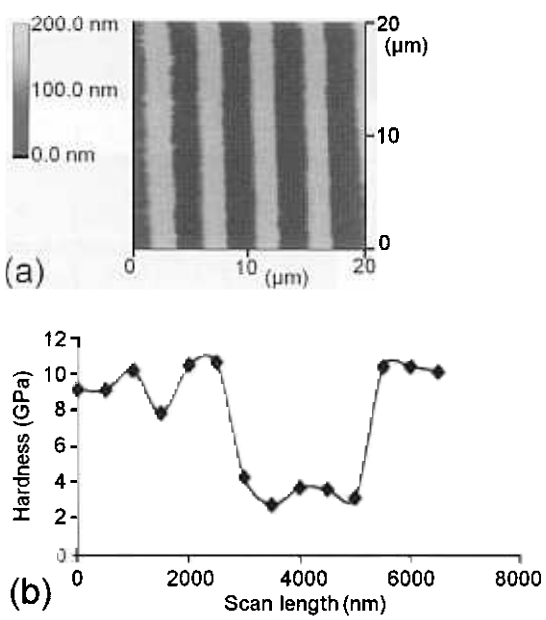

Fig. 8. AFM image (a) of the Ni–Al structured sample, and (b) the corresponding hardness distribution along the scan length in one period. The line is only indicative [31].

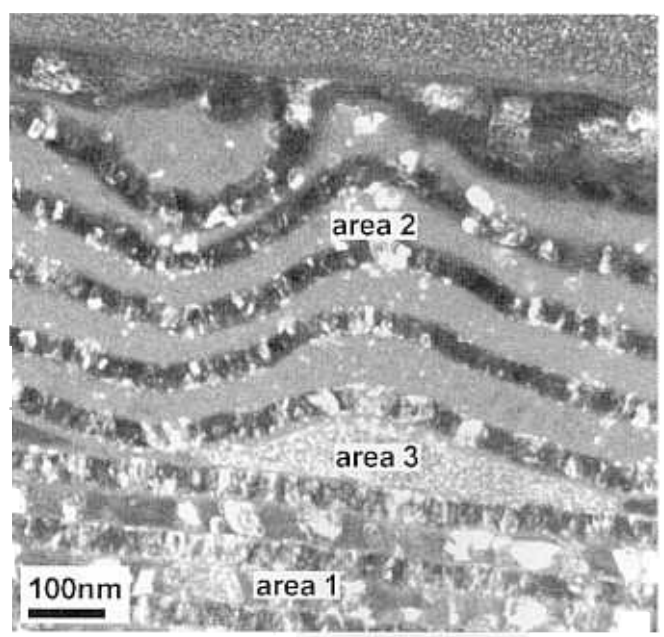

Fig. 9. Cross-sectional TEM image (dark field) of an area exposed to laser interference maximum. The microstructure in the individual Al sublayers appears to be fine grained in area 2 (5 to 10 nm), one large grain in the area 3 (> 100 nm), and unchanged nano-grained structure in the rest of the sample named area 1 (20 to 30 nm) [32].

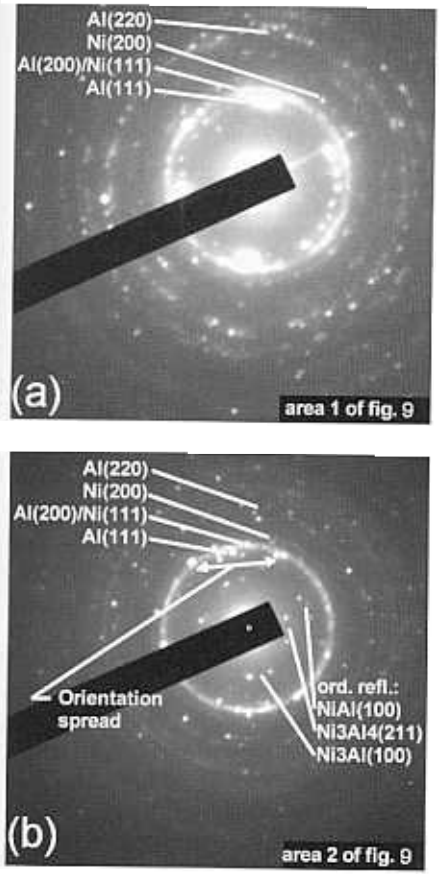

Fig. 10. TEM diffraction images: (a) un-irradiated layers without ordered intermetallics' reflexes and a strong fiber texture (Fig. 8, area 1); (b) strongly irradiated layers with ordered intermetallics' reflexes and a texture change with an orientation spread (Fig. 8, area 2) [32].

Figure 10 shows two electron diffraction images on different sample positions. A strong texture in the film can be seen (Fig. 10a). Such a texture is normal for PVD produced films. The texture and phase-microstructure changes after laser interference irradiation depending on the depth. The deformation of Ni layers described tilts the crystals in preferred directions perpendicular to the line-like interference structure and generates an orientation spread in the electron diffraction image (Fig. 10b). This could also explain the hardness change as the resulting Ni texture is mechanically more stable than before irradiation.

The diffraction image of unchanged layers (Fig. 10a) shows only Ni and Al reflexes but not ordered intermetallics' reflexes. In the first two bi-layers, inter-diffusion between Ni and Al resulting from the temperature-driven change of the diffusion coefficient and the deformation of layers can be seen. In this way, the formation of intermetallics is initiated by the laser interference irradiation. This is shown in Fig. 10b where the higher ordered intermetallics' reflexes of NiAl, Ni_3Al_4, and Ni_3Al are observed. In Fig. 10b, an orientation spread of the Al(200)/Ni(111) reflexes similar to the X-ray diffraction measurements in [29] can be seen.

6.3. Scaling of mechanical behavior

A structural change that results in a property change can be initiated by the laser fluence exceeding a certain threshold value. Line-type periodical structures are comparable to

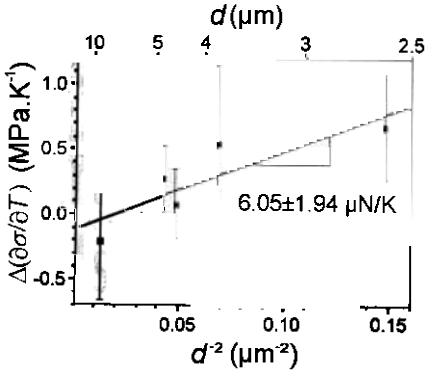

Fig. 11. Resulting scaling behavior of substrate/film system due to Laser Interference Metallurgy. The change in thermoelastic slope measured with the substrate curvature technique is a function of the periodicity d [36].

composites such as lamellar structures in bones [35]. A significant increment of the elastic modulus and hardness under the laser intensity peaks was measured and explained by changes in the grain size, which result from the high cooling rate at the interference maxima (about $10^{10}\,K \cdot s^{-1}$) together with local phase changes [36]. In [36], the macroscopic effects in thin films produced by Laser Interference Metallurgy were discussed. The results demonstrate that local and periodic changes of the mechanical properties due to the microstructural manipulation of the samples results in a macroscopic stiffness effect [36]. Using the mechanical laminar theory, it was proven that the stiffness effect is a function of the structure period d as shown in Fig. 11. The demonstrated scaling behavior of the multilayered Ni/Al system was higher than that achieved by a biological bone-like hierarchical structure.

7. Conclusions

The Laser Interference Metallurgy method allows the creation of several kinds of surface arrays with a well-defined long range order in the scale of the microstructure. Due to the strong interaction of the laser energy with the surface of metals and with deposited metallic layers it can serve for direct patterning of phases and various microstructural features with well known metallurgical effects such as melting, recrystallization, quenching, recovery and defect and phase formation, achieved laterally at a micro-scale.

Different aspects of Laser Interference Metallurgy were discussed. The formation of complex periodical structures in thin metallic film samples by using three laser beams with uniform and non-uniform intensity was demonstrated and explained theoretically by means of laser interference theory. Moreover, a method to calculate, prior to the experiments, the number and geometrical arrangement of the laser beams needed to obtain a desired periodical pattern was explained. The microstructural changes (namely morphology, grain size distribution, texture, and phase microstructure) in multi-layered metallic thin films were described. These changes have been demonstrated to be responsible for macroscopic and micrometer-scaled periodical changes of mechanical properties. If the structure is realized on a nanometer-scaled multi-film, a two step hierarchical bio-mimetic composite structure can be obtained.

The authors greatly acknowledge the scholarships awarded to A. Lasagni by the DFG Graduiertenkolleg GRK 232/3-2 and the Deutscher Akademischer Austausch Dienst (DAAD). The research work of Prof. Mücklich was supported by the Alfried Krupp Prize for Young University Teachers awarded by the Krupp Foundation. C. Daniel is a research staff member and Eugene P. Wigner Fellow at Oak Ridge National Laboratory managed by UT-Battelle, LLC for the Department of Energy under contract DE-AC05-00OR22725.

References

[1] P.B. Clapham, M.C. Hutley: Nature (1973) 281.
[2] S.J. Wilson, M.C. Hutley: Optica Acta 29 (1982) 993.
[3] S. Weiner, W. Traub, H.D. Wagner: J. Struct. Biol. 126 (1999) 241.
[4] X. Xia: Adv. Mater. 16 (2004) 1245.
[5] M. Geissler, X. Xia: Adv. Mater. 16 (2004) 15, 1249.
[6] C. David, A. Souvorov: Review of Scientific Instruments 70, no. 11 (1999) 4168.
[7] B.H. Cumpston, S.P. Ananthavel, S. Barlow, D.L. Dyer, J.E. Ehrlich, L.L. Erskine, A.A. Heikal, S.M. Kuebler, I.-Y. S. Lee, D. McCord-Maughon, J. Qin, H. Rockel, M. Rumi, X.-Li Wu, S.R. Marder, J.W. Perry: Nature 398 (1999) 51.
[8] R. Jakubiak, T.J. Bunning, R.A. Vaia: Nanotechnology E-Bulletin, 1.1 (2004) 3.
[9] F. Mücklich, A. Lasagni, C. Daniel: Intermetallics 13 (2005) 437.
[10] A. Blatter, M. Maillat, S.M. Pimenov, G.A. Shafeev, A.V. Simakin: Trib. Lett. 4 (1998) 237.
[11] H.M. Phillips, D.L. Callahan, R. Sauerbrey, G. Szabó, Z. Bor: Appl. Phys. Lett. 58 (1991) 2761.
[12] M. Heintze, P.V. Santos, C.E. Nebel, M. Stutzmann: Appl. Phys. Lett. 64 (1994) 3148.
[13] M.K. Kelly, J. Rogg, C.E. Nebel, M. Stutzmann, S. Kátai: Phys. Stat. Sol. (a) 166 (1998) 651.
[14] H. Fukumura, Y. Kohji, K. Nagasawa, H. Masuhara: J. Am. Chem. Soc. 116 (1994) 10304.
[15] S. Shoji, S. Kawata: Appl. Phys. Lett. 76 (2000) 2668.
[16] A. Lasagni, M. Seyler, C. Holzapfel, W. Maier, F. Mücklich: Adv. Mater. 17 (2005) 2228.
[17] C. Daniel, F. Mücklich, Z. Liu: App. Surf. Sci. 208–209 (2003) 317.
[18] C. Daniel, F. Mücklich: Wear 257 (2004) 3–4, 266.
[19] S.M. Metev, V.P. Veiko: Laser-Assisted Micro-Technology, second edition, Springer Berlin, Germany, 1998.
[20] A. Lasagni, C. Holzapfel, F. Mücklich: Adv. Eng. Mater. 7 (2005) 6, 487.
[21] M. Mützel, U. Rasbach, D. Meschede, C. Burstedde, J. Braun, A. Kunoth, K. Peithmann, K. Buse: Appl. Phys. B 77 (2003) 1.
[22] U. Drodofsky, J. Stuhler, T. Schulze, M. Drewsen, B. Brezger, T. Pfau, J. Mlynek: Appl. Phys. B 65 (1997) 755.
[23] A. Lasagni, C. Holzapfel, F. Mücklich, in: S.J. Bull, P.R. Chalker, S. Chen Chen, W.J. Meng, R. Maboudian (Eds.), Proc. Mat. Res. Soc. Symp. 890-Y04, 02.1.
[24] S. Lipson, H. Lipson, D. Tannhauser: Optik, 3rd edition, Springer, Germany, 1997, 171.
[25] A. Lasagni, F. Mücklich: Appl. Surf. Sci. 240 (2005) 214.
[26] A. Lasagni, F. Mücklich: Appl. Surf. Sci. 247 (2005) 32.
[27] A. Lasagni, C. Holzapfel, F. Mücklich: Appl. Surf. Sci. (accepted)
[28] A. Lasagni, F. Mücklich: Prakt. Metallogr. 43 (2006) 1, 16.
[29] C. Daniel, A. Lasagni, F. Mücklich: Surf. and Coat. Technol. 180–181 (2004) 478.
[30] X.K. Meng, H. Vehoff: J. Mater. Res. 15 (2000) 2596.
[31] Z. Liu, X.K. Meng, T. Recktenwald, F. Mücklich: Mat. Sci. Eng. A 342 (2003) 101.
[32] C. Daniel, F. Mücklich: App. Surf. Sci. 242 (2005) 140.
[33] S. Tamirisakandala, P.V.R.K. Yellapregada, S.C. Medeiros, W.G. Frazier, J.C. Malas, B. Dutta: Adv. Eng. Mater. 5 (2003) 667.
[34] KW. Liu, F. Mücklich, in: G.A. Nazri, M. Nazri, R. Young, P. Chen (Eds.), Mat. Res. Soc. Symp. Vol. 2003;753:BB6.5
[35] I. Jäger, P. Fratzl: Biophys. J. 79 (2000) 1737.
[36] C. Daniel, T.J. Balk, T. Wübben, F. Mücklich: Adv. Eng. Mater. 7 (2005) 9, 823.

(Received March 22, 2006; accepted July 6, 2006)

Correspondence address

Prof. Dr.-Ing. Frank Mücklich
Functional Materials Lab., Dept. Materials Science
Saarland University, P.O. Box 151150
D-66041 Saarbrücken, Germany
Tel.: +49 681 302 2048
Fax: +49 681 302 4876
E-mail: muecke@matsci.uni-sb.de

You will find the article and additional material by entering the document number MK101375 on our website at www.ijmr.de